PHYSICAL REVIEW A **68**, 010701(R) (2003)

Large-angle elastic resonant and nonresonant scattering of electrons from $B^{3+}(1s^2)$ and $B^{4+}(1s)$ ions: Comparison of experiment and theory

T. J. M. Zouros,[1,*] E. P. Benis,[2] and T. W. Gorczyca[3]
[1]*Department of Physics, University of Crete and IESL-FORTH, P.O. Box 2208, 71003 Heraklion, Crete, Greece*
[2]*J.R. Macdonald Laboratory, Department of Physics, Kansas State University, Manhattan, Kansas 66506-2604, USA*
[3]*Department of Physics, Western Michigan University, Kalamazoo, Michigan 49008-5252, USA*
(Received 20 September 2002; published 17 July 2003)

High-resolution doubly differential cross section measurements and calculations for electrons elastically scattered through 180° from ground-state He- and H-like boron ions are presented covering the entire $1s2lnl'$ (for B^{3+}) and $2lnl'$ (for B^{4+}) Rydberg series populated by resonant excitation. The measurements were performed by zero-degree Auger projectile electron spectroscopy of 4-MeV $B^{3+,4+}$ ions in collisions with H_2 targets. *R*-matrix calculations, particularly sensitive at this large scattering angle to electron correlation, exchange, and interference effects, are found to be in excellent overall agreement within the electron-scattering model.

DOI: 10.1103/PhysRevA.68.010701 PACS number(s): 34.80.Lx

Electron-ion differential scattering measurements probe the delicate interactions between the electron, the short-range scattering potential due to the electronic structure of the ion, and the long-range Coulomb potential due to the ion's charge [1]. Thus, not only do they provide sensitive tests of the structure and dynamics of electron-ion scattering, but they also find important applications in the extensive modeling of fusion and astrophysical plasmas, x-ray lasers, and electron cooling of highly charged ions (HCI) in storage rings [1,2].

Small-angle ($\theta \lesssim 80°$) electron scattering [3,4] corresponds to distant collisions. Therefore, it is dominated by the ionic Coulomb potential, exhibits the well-known Rutherford scattering behavior, and is well understood [1]. Large-angle ($\theta \gtrsim 80°$) scattering [5] corresponds to a deeper probing of the atomic structure near the distance of closest approach. It is, therefore, much more sensitive to correlation, exchange [1,3–5], bound-state resonances, and interference effects [1,6–8], especially at the largest scattering angles around $\theta = 180°$ [6,4]. These effects are particularly enhanced in electron-ion collisions, since there are many more bound channels available compared to those in electron-atom scattering [1].

Electron scattering from HCI with just a few electrons, such as H-like and He-like ions, offers some of the simplest testing grounds of atomic structure and collision theory. Short-lived bound-state resonances populated by resonant excitation (RE) give rise to the formation of doubly excited, two- and three-electron states, respectively. In RE, the ionic electron is excited, while the scattering electron is captured, in a process equivalent to the time-reversed Auger process. These resonances can then relax either by photon or electron emission, in which case the process is known as dielectronic recombination (DR) or resonant elastic scattering, respectively. *Total* cross sections have been determined for DR ($\Delta n = 0$ from metastable $O^{6+}(1s2s\,^{3,1}S)$ [9], $\Delta n = 1$ from $O^{7+}(1s)$ [10] and ground state $C^{4+}(1s^2)$ [11]), as well as from other HCI [2], primarily in ion storage rings with very high precision, by extracting the final charge-changed ions. However, they do not include interference from cross terms (see below), which can only be fully investigated by *differential electron-scattering* measurements. Such experiments, however, are tedious, involving low luminosity crossed or merged beams. Only a handful of such differential cross sections have been measured [1,3–5], for scattering angles $\theta \lesssim 150°$, while *no* resonances have ever been traced out in any type of merged or crossed-beam electron-ion differential scattering experiment.

Quasifree electron-ion differential scattering measurements exploit the $\sim 10^8$ times more luminosity available in collisions between *lightly bound* target electrons and energetic HCI. This approach, refined over the last decade [12–14] by substantially reducing undesirable *nucleus-ion* contributions using favorable collision conditions and low-*Z* targets [14,15], has evolved into what is known as the electron-scattering model (ESM) [7,12,16–18]. Recent good agreement with *R*-matrix calculations have caught the attention of the electron-ion scattering community [1,2] and include measurements of resonant and nonresonant elastic [13,19] and inelastic [16,20] electron scattering from H-like ions, as well as superelastic scattering from metastable He-like ions [21,22].

Resonant elastic-scattering investigations have focused primarily on the $2p^2\,^1D$ state, the *single* strong RE line seen in the $2lnl'$ Rydberg series of H-like ions [19]. This only tests calculations over the very narrow energy range of a few eV. Opening up the much richer resonance structure of the RE $1s2lnl'$ Rydberg series [11] by scattering from *ground-state* He-like ions would allow for a much more extensive testing of theory. However, such differential scattering measurements have *never* been performed, primarily because He-like ions usually include a large fraction of $1s2s\,^3S$ metastable states f_{3S}[23,24], which is hard to measure directly.

Here, we report on the first *absolute* doubly differential cross-section (DDCS) measurements and calculations for 180° elastic (resonant and nonresonant) quasifree electron scattering from ground-state He-like $B^{3+}(1s^2)$ ions. These results extend over the full $1s2lnl'$ Rydberg series, covering

*Email address: tzouros@physics.uoc.gr

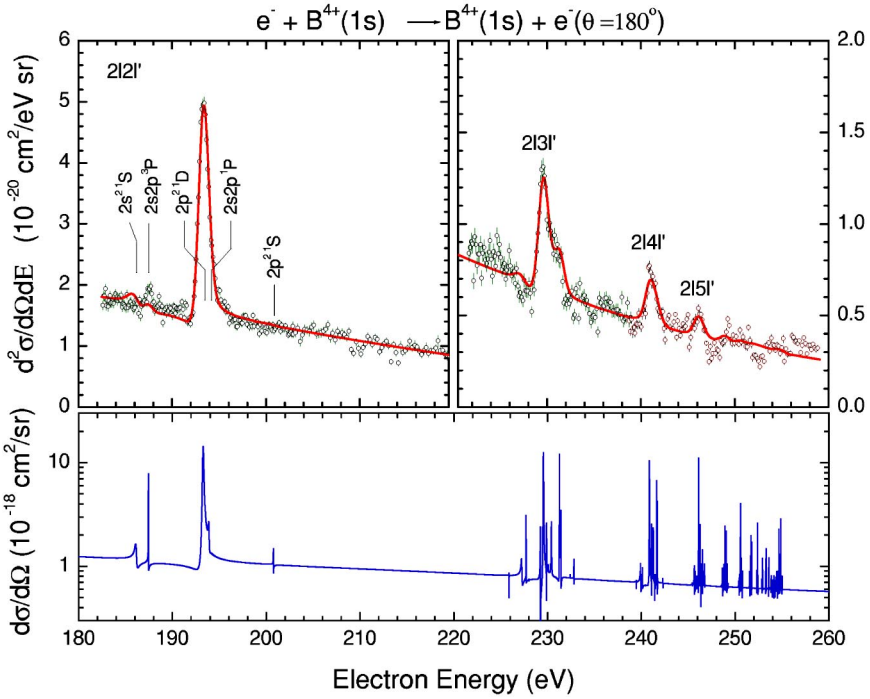

FIG. 1. (Color online) DDCSs for 180° elastic electron scattering from B^{4+}. The entire $2lnl'$ Rydberg series range is covered. Data: Zero-degree electron spectra for 3.91-MeV $B^{4+}+H_2$ collisions. Error bars are due to statistics only. Theory: *R*-matrix results (bottom) within the ESM [see Eq. (2)] and after convolution with a 0.5-eV Gaussian representing the spectrometer resolution (top).

a wide electron energy range from 150 to 205 eV. They, thus, provide an extensive test of differential elastic electron-ion scattering calculations and the ESM. The He-like boron ions were produced at 4 MeV by extracting them directly from the tandem accelerator without subsequent poststripping. This procedure was found to strongly suppress the undesirable metastable beam component to the negligible amount of $f_{^3S}=(3\pm1)\%$, which was determined using the newly developed *in situ* technique [24] enabling a very accurate absolute DDCS determination. An additional consistency check was provided by scattering from the simpler H-like $B^{4+}(1s)$ ions. These DDCSs did not only include the strong $2p^{2\,1}D$ resonance, already well known for free [10] and quasifree [7,19] electron scattering from other H-like ions, but also the weaker, higher-lying members of the $2lnl'$ Rydberg series of RE states, never measured to date. Both measurements were made possible due to a newly developed, high efficiency zero-degree Auger projectile spectroscopy (ZAPS) apparatus [25]. Finally, *R*-matrix calculations were performed and used within the ESM framework resulting in excellent overall agreement with both H-like and He-like measurements.

In the ESM, the *bound* target electron, as seen from the rest frame of the ion, is considered to interact as a *free* electron, with its velocity distribution given by its Compton profile $J(v_z)$ [17]. Thus, the velocity of the impinging quasifree electron $\vec{V}$ is related to the ion velocity $\vec{V}_p$ by the frame transformation $\vec{V}=\vec{V}_p+\vec{v}$. The velocity $\vec{v}$ of the electron due to its bound motion around the target atom and E, its kinetic energy in the ion rest frame, are related (in atomic units) by [12,18]

$$E=\tfrac{1}{2}(\vec{V}_p+\vec{v})^2-E_I\approx\tfrac{1}{2}V_p^2+v_zV_p+\tfrac{1}{2}v_z^2-E_I, \qquad (1)$$

where E_I is the ionization potential of the target electron. The components of $\vec{v}$ perpendicular to $\vec{V}_p=V_p\hat{z}$, which are assumed to be much smaller than V_p, are neglected [18].

The free electron-ion scattering singly differential cross section (SDCS) is then related to the quasifree electron-ion scattering DDCS by [12,18]

$$\left.\frac{d^2\sigma(E,\theta)}{d\Omega\,dE}\right|_{quasifree}=\left.\frac{d\sigma(E,\theta)}{d\Omega}\right|_{free}\frac{J(v_z)}{V_p+v_z}. \qquad (2)$$

For H_2 targets, analytic expressions of $J(v_z)$ have been fitted to high-energy electron-impact measurements [19].

The theoretical elastic electron-scattering SDCS $d\sigma(E,\theta)/d\Omega$ was obtained using an *R*-matrix method. First, for the B^{3+} calculation, a basis set of physical orbitals $nl=\{1s,2s,2p,3s,3p,3d\}$ was determined from $1snl$ configuration-averaged Hartree-Fock calculations [26]. Then all *N*-electron configurations $nln'l'$ were used to describe the 11 lowest states of B^{3+}: $1s^{2\,1}S$, $1s2s\,^{1,3}S$, $1s2p\,^{1,3}P$, $1s3s\,^{1,3}S$, $1s3p\,^{1,3}P$, and $1s3d\,^{1,3}D$. A basis of 40 additional orthogonal orbitals was coupled to these 11 configuration-interaction target states to represent the resonance or continuum wave functions of B^{2+}. To compensate for the necessary orthogonality and to include extra correlation, all $(N+1)$-electron configurations $nln'l'n''l''$ were also included here. (For the B^{4+} calculation, hydrogenic orbitals $nl=\{1s,2s,2p,3s,3p,3d\}$ were used to describe exactly the lowest six states of B^{4+}, 40 additional orbitals were coupled to these to describe the resonance or continuum wave functions of B^{3+}, and all $(N+1)$-electron configurations $nln'l'$ were also included.)

With this atomic structure, the *R*-matrix suite of codes [27] was utilized to compute scattering transition matrices $T_{i\to f}(E)$. For the present investigation, a new code, based closely on the work of Griffin and Pindzola [6], was developed to compute the differential cross section at each energy

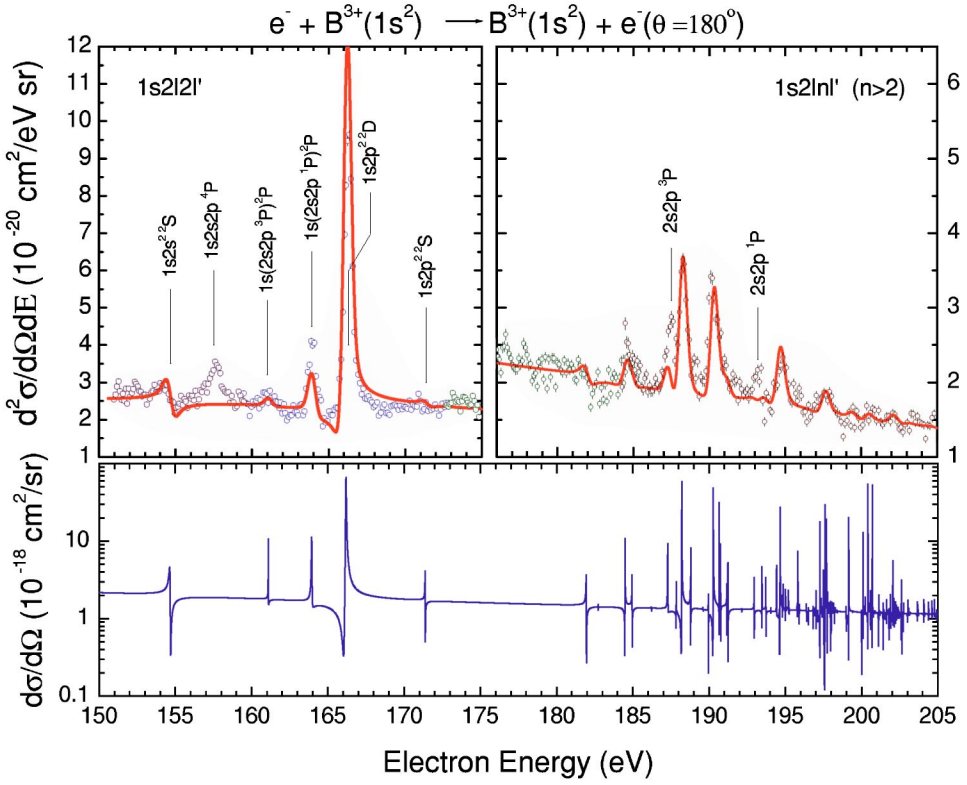

FIG. 2. (Color online) As for Fig. 1, but for 4.0-MeV $B^{3+}(1s^2)$. The entire $1s2lnl'$ Rydberg series range is covered.

E from Eq. (4) in Ref. [6]. Since that expression involves *cross terms* between lower and higher partial-wave symmetries L, it was necessary to include *more* partial waves than were needed to converge the total cross section (which does not involve cross terms); partial waves up to $L_{max}=9$ were used. A final convolution with the analyzer resolution enabled a direct comparison to the data using Eq. (2).

The electron spectra were measured at the 7-MV EN tandem Van de Graaff accelerator facility of the J. R. Macdonald laboratory at Kansas State University. The ZAPS apparatus incorporated a single-stage hemispherical analyzer (mean radius 101.6 mm, full width at half maximum (FWHM) energy resolution 0.15%) with a 40-mm two-dimensional position sensitive detector having a 20% energy bandwidth [25] and a full angular acceptance of 0.868°. The electron spectra were converted to *absolute* DDCS by normalizing to the 180° elastic electron-scattering (Rutherford) differential cross section. The normalization factor was obtained from the Binary Encounter electron (BEe) [18] spectra in 13-MeV B^{5+} collisions with H_2 with an overall absolute uncertainty of about 20% for *all* measured DDCSs. In a final step, the DDCSs were converted to the ion rest frame, where they were directly compared to theory.

In Figs. 1 and 2, the $B^{3+}(2lnl')$ and $B^{2+}(1s2lnl')$ doubly excited states are shown lying on top of the broad nonresonant elastic-scattering continuum. These lines are predominantly formed by RE followed by Auger decay back to the ground state. In the corresponding R-matrix calculations, interference signatures are evident in the many ''dips'' of the calculated SDCSs. The overall agreement is seen to be remarkably good, considering there are no adjustable parameters. Inclusion of radiation damping was found to be unnecessary.

For B^{4+}, the excellent agreement with the calculation indicates that the ESM is still valid, even at this rather low collision velocity, $V_p=3.8$ a.u. For B^{3+}, some substantial Fano interference structures [28] are predicted by the calculation at 155 and 166 eV, but are only barely observable with the existing energy resolution. However, some discrepancy seems to be evident, in the vicinity of the $1s(2s2p\,^1P)^2P$ and $1s2p^2\,^2D$ lines between 163 and 170 eV. Since our R-matrix results were found to be fairly insensitive to further inclusion of configuration interaction and pseudo-orbitals (optimized on the actual $1s2l2l'$ configuration), we rule out an unconverged theoretical description of the scattering processes as the cause for this discrepancy. We also rule out RE contributions to the B^{2+} KLL lines from the small $B^{3+}(1s2s\,^3S)$ contaminant, since these energy levels lie above the $B^{2+}(1s2l2l')$ levels [23]. Note, however, the observed $1s2s2p\,^4P$ and $2s2p\,^{3,1}P$ Auger lines, which are populated by electron capture and $1s\rightarrow 2p$ excitation of the $B^{3+}(1s2s\,^3S)$ metastable component of the beam, respectively, and are not included in the calculation. The former observation guarantees that the two $1s2s2p\,^2P$ states will also be populated (an analysis of the capture of an uncoupled $2p$ electron to the $1s2s\,^3S$ state shows that the relative populations of the $1s2s2p\,^4P$, $1s(2s2p\,^3P)^2P$, and $1s(2s2p\,^1P)^2P$ states will be in the ratio of 8:1:3). These additional ^2P contributions are the reason that the R-matrix results do not line up perfectly with experiment in the 163–170 eV region. As a final note, the ratio of the ^4P to ^2D line

intensities is proportional to the fraction f_{3S}, since the ^4P state is produced from the $1s2s\,^3S$ state and the ^2D state from the $1s^2\,^1S$ state, respectively. The ^4P line is thus important for the *in situ* determination of f_{3S} [24].

We would also like to emphasize that the effective *broad* energy distribution of the quasifree electron ''beam'' (a few hundred eV in FWHM) is actually *advantageous* [16]. Particularly in measuring DDCSs, the whole series of RE states can be brought into resonance *simultaneously* at 4 MeV, albeit with some minor reduction in intensity, as dictated by the Compton profile $J(v_z)$. Furthermore, as $J(v_z)$ is just an overall scaling factor within the ESM [Eq. (2)], no deconvolution of its influence on the DDCSs is needed, as in the case of excitation or ionization [14].

The excellent overall agreement between *R*-matrix calculations and the present measurements, at the DDCS level and over a broad energy range with many resonances, for collisions with both H-like and He-like boron, represents a milestone in the testing of the ESM. The ESM is important as it provides a simple and general framework for linking electron-scattering processes in the two rather distinct fields of ion-atom and ion-electron collisions [14]. The realization that the ion-atom collision processes of resonance transfer and excitation (RTE) [29], followed by Auger emission (RTEA) and BEe [12,18] production (and their possible interference), could be treated within the ESM on the *same* footing as quasifree elastic resonant electron scattering (for RTEA) and nonresonant electron scattering (for BEe) from HCI, led to the use of the powerful electron-scattering *R*-matrix technique to describe RTEA and BEe, and with it the evolution in nomenclature reflecting this deeper understanding [12,13,16,19–22].

In summary, we present the most extensive tests of elastic differential electron-ion scattering, to date, by measuring absolute DDCSs for quasifree electron backscattering from ground-state He-like and H-like boron ions over a wide energy range. A new, high-efficiency, zero-degree Auger projectile spectrograph, combined with a novel technique to obtain practically pure ground-state He-like boron ions, allowed for accurate DDCS measurements. A new *R*-matrix calculation for elastic, resonant, and nonresonant, 180° differential cross sections for scattering of electrons from boron ions was found to be in excellent overall agreement. These results add to the mounting evidence [2,12] that quasifree electron scattering, combined with high-resolution Auger projectile spectroscopy techniques, can be used to obtain unique, large-angle scattering DDCSs of electrons from HCI. Since such measurements cannot be readily performed by conventional crossed or merged electron-ion differential scattering experiments, they presently provide the only viable technique for testing electron-ion differential scattering calculations, particularly in the sensitive large-angle scattering regime.

We thank Pat Richard for stimulating discussions and Don Griffin for invaluable contributions on the angular differential aspects of this investigation. This work was supported by the Division of Chemical Sciences, Geosciences and Biosciences, Office of Basic Energy Sciences, Office of Science, U.S. Department of Energy. T.W.G. was supported in part by NASA Space Astrophysics Research and Analysis Program Grant No. NAG5-10445.

[1] I.D. Williams, Rep. Prog. Phys. **62**, 1431 (1999), and references therein.
[2] A. Müller, in *Atomic and Molecular Data and their Applications*, edited by David R. Schultz, Predrag S. Krstic, and Fay Ownby, AIP Conf. Proc. No. **636** (AIP, Melville, NY, 2002), 202–212, and references therein.
[3] B.A. Huber *et al.*, Phys. Rev. Lett. **73**, 2301 (1994).
[4] J.B. Greenwood, I.D. Williams, and P. McGuinness, Phys. Rev. Lett. **75**, 1062 (1995).
[5] C. Bélenger *et al.*, J. Phys. B **29**, 4443 (1996).
[6] D.C. Griffin and M.S. Pindzola, Phys. Rev. A **42**, 248 (1990).
[7] C.P. Bhalla, Phys. Rev. Lett. **64**, 1103 (1990).
[8] G.X. Chen and A.K. Pradhan, Phys. Rev. Lett. **89**, 013202 (2002).
[9] L.H. Andersen, P. Hvelplund, H. Knudsen, and P. Kvistgaard, Phys. Rev. Lett. **62**, 2656 (1989).
[10] G. Kilgus *et al.*, Phys. Rev. Lett. **64**, 737 (1990).
[11] G. Kilgus *et al.*, Phys. Rev. A **47**, 4859 (1993).
[12] P. Richard, C.P. Bhalla, S. Hagmann, and P. Zavodszky, Phys. Scr., **T80B**, 87 (1999), and references therein.
[13] C. Liao *et al.*, Phys. Rev. A **59**, 2773 (1999).
[14] T.J.M. Zouros, Comments At. Mol. Phys. **32**, 291 (1996), and references therein.
[15] T.J.M. Zouros and D.H. Lee, in *Accelerator-Based Atomic Physics Techniques and Applications*, edited by S.M. Shafroth and J.C. Austin (AIP Press, Woodbury, NY, 1999), pp. 426–479, and references therein.
[16] P. Hvelplund, A.D. Gonzalez, P. Dahl, and C.P. Bhalla, Phys. Rev. A **49**, 2535 (1994).
[17] D. Brandt, Phys. Rev. A **27**, 1314 (1983).
[18] D.H. Lee *et al.*, Phys. Rev. A **41**, 4816 (1990).
[19] G. Toth *et al.*, Phys. Scr., T **T92**, 272 (2001).
[20] P. Závodszky *et al.*, J. Phys. B **32**, 4425 (1999).
[21] P. Závodszky *et al.*, Phys. Rev. Lett. **87**, 033202 (2001).
[22] A. Alnaser *et al.*, Phys. Rev. A **65**, 042709 (2002).
[23] D.H. Lee *et al.*, Phys. Rev. A **44**, 1636 (1991).
[24] E.P. Benis, M. Zamkov, P. Richard, and T.J.M. Zouros, Phys. Rev. A **65**, 064701 (2002).
[25] E.P. Benis, T.J.M. Zouros, H. Aliabadi, and P. Richard, Phys Scr., **T80B**, 529 (1999).
[26] C. Froese-Fischer, Comput. Phys. Commun. **64**, 369 (1991).
[27] K.A. Berrington, W.B. Eissner, and P.H. Norrington, Comput. Phys. Commun. **92**, 290 (1995).
[28] U. Fano, Phys. Rev. **124**, 1866 (1961).
[29] See reviews by T.J.M. Zouros and J.A. Tanis in *Recombination of Atomic Ions*, *NATO Advanced Studies Institute, Series B: Physics*, edited by W.G. Graham, W. Fritsch, Y. Hahn and J.A. Tanis (Plenum, New York, 1992), pp. 217–300 and 241–257, and references therein.